THE JOURNAL OF PHYSICAL CHEMISTRY B

Article

pubs.acs.org/JPCB

Multi-Scale Simulation of the Simian Immunodeficiency Virus Fusion Peptide

Jean-Marc Crowet,*[,†] Daniel L. Parton,[‡,§] Benjamin A. Hall,[‡,∥] Sven Steinhauer,[†] Robert Brasseur,[†] Laurence Lins,[†,#] and Mark S. P. Sansom[‡,#]

[†]Centre de Biophysique Moléculaire Numérique, Gembloux Agro-Bio Tech, University of Liège, 2 Passage des déportés, B-5030 Gembloux, Belgium

[‡]Department of Biochemistry, University of Oxford, South Parks Road, Oxford, OX1 3QU, United Kingdom

Supporting Information

ABSTRACT: Fusion peptides of type I fusion glycoproteins are structural elements of several enveloped viruses which enable the fusion between host and virus membranes. It is generally suggested that these peptides can promote the early fusion steps by inducing membrane curvature and that they adopt a tilted helical conformation in membranes. Although this property has been the subject of several experimental and in silico studies, an extensive sampling of the membrane peptide interaction has not yet been done. In this study, we performed coarse-grained molecular dynamic simulations in which the lipid bilayer self-assembles around the peptide. The simulations indicate that the SIV fusion peptide can adopt two different orientations in a DPPC bilayer, a major population which adopts a tilted interfacial orientation and a minor population which is perpendicular to the bilayer. The simulations also indicate that for the SIV mutant that does not induce fusion in vitro the tilt is abolished.

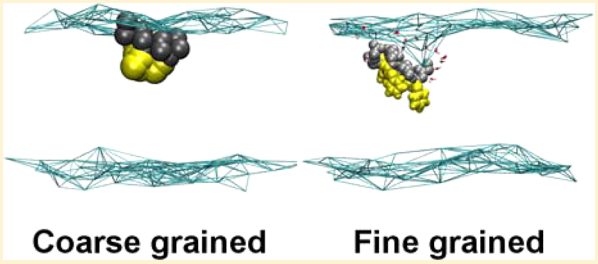

INTRODUCTION

Like all enveloped viruses, Simian immunodeficiency virus (SIV) initiates infection by fusing its envelope with the target cell membrane.[1] This fusion is mediated by a trimeric glycoprotein (gp) complex made of two subunits, a surface glycoprotein, responsible for the binding to specific cell receptor(s) and a transmembrane glycoprotein, directly involved in the fusion process. These subunits are gp120 and gp32, respectively, for SIV and come from the proteolytic cleavage of the glycoprotein precursor gp160.[2,3] Gp32 is a class I fusion glycoprotein, like those of HIV, Influenza, and Ebola virus, for which cleavage generates a new N-terminal extremity corresponding to the fusion peptide (FP). These peptides usually correspond to hydrophobic segments enriched in Gly residues and whose mutation generally leads to a loss of activity[4] supporting their direct involvement in the fusion process.[5] Moreover, synthetic peptides corresponding to FP sequences usually destabilize membrane bilayers as evidenced by lipid mixing experiments.[4,6] Several functions have been proposed for these fragments, such as acting as anchors to join the viral and cell membranes or lowering the rupture tension of the lipid monolayer, but it is generally suggested that they can promote the early fusion steps by inducing membrane curvature.[4,7]

When inserted into membranes, structure and/or orientation of synthetic FP can notably be determined by techniques such as infrared spectroscopy (ATR-FTIR) or neutron diffraction. It has been found that many FP are inserted at an oblique angle.[8,9] A tilted orientation for FP has first been predicted by molecular modeling in 1987 for the Newcastle Disease Virus (NDV)[10] and since then for other FPs such as that of SIV,[11] HIV,[12] HA2,[13,14] or BLV.[15] These tilted peptides (TP) present an asymmetric distribution of their hydrophobic amino acids when helical, resulting in a hydrophobicity gradient.[16,17] Because of the gradient, they adopt an oblique orientation toward a hydrophobic/hydrophilic interface (such as biological membranes) which is thought to disturb the parallelism of lipid acyl chains.[14,18,19] Although the FP structure relevant for fusion is generally reported as helical, there is also evidence for an extended conformation, notably for HIV.[20−22] However, Li et al. showed that lipid mixing occurs at peptide/lipid ratios that support the helical structure.[23] Structural plasticity of FP has been highlighted by several studies, and both structures could be important at different steps of the fusion process.[24,25] For example, FPs could oligomerize as β-sheet structures during the formation of the fusion pore.[4,5]

The predicted tilted peptides are generally associated with fusion and leakage of liposomes experimentally[16,17,26,27] and hence with membrane destabilization. Structural approaches, like polarized infrared spectroscopy (ATR-FTIR), have shown that the fusion depends on the helix formation and orientation into lipid bilayers.[28−30] Nontilted mutants designed in silico lose their fusion activity, while mutations that restore the tilt also restore the fusogenic activity.[8,29,31] This holds true for

Received: March 22, 2012
Revised: October 24, 2012
Published: October 25, 2012

dx.doi.org/10.1021/jp3027385 | J. Phys. Chem. B 2012, 116, 13713−13721

mutations made on the whole protein.[8,15] These results support the biological relevance of tilted peptides.[5] Finally, effects of mutations described in the literature have been compared to in silico and in vitro results: a good correlation is noticed, as reviewed by Charloteaux et al.[5] These data suggest that the tilted orientation is implicated in the lipid destabilizing activity of FP.[18,32,33] Furthermore, the tilted insertion will increase the volume at the lipid tails level which could in turn promote a negative curvature of the membrane.[34]

Besides ATR-FTIR, tilted insertion of FP has also been observed by other experimental techniques. Bradshaw et al. determined from a neutron diffraction study on the deuterated SIV fusion peptide in a DOPC multilayer that the most probable orientation corresponds to an angle of 55° with respect to the bilayer normal.[35] Han et al. determined a kinked structure for the fusion domain of Influenza hemagglutinin HA2 in DPC micelles by using NMR and EPR distance constraints. Due to conformational changes, the N-terminal helix inserts at an angle of 38° at pH 5 (instead of 23° at pH 7.4), corresponding to the fusogenic conditions.[36]

Several molecular dynamic studies have been carried on fusion peptides[32,37,38] in order to decipher their structure and mode of insertion as well as the membrane composition effects. Kamath et al. (2002) simulated the HIV FP (16aa) in a preformed POPE bilayer for 1.4 ns and found that, contrary to nonfusogenic mutants who lie on the bilayer surface, the WT peptide adopts a 44 ± 6° angle and increases the thickness of the interfacial area.[32] The studies of this group as well as others carried on HA2 FP support the tilted orientation of FPs as helices into bilayer and their implication in the fusion process.[32,37−43] In the simulations of Kasson et al., the HA2 FP also significantly increases the lipid tail protusion within 5 Å of the peptide.[44] A more general study carried on several fusion peptides from HIV, Rubella, Newcastle, and so forth has recently been conducted and also supports this statement. Moreover, they brought a physical explanation for the tilt insertion and the depth of penetration in an explicit DMPC bilayer, notably by the lipophilicity repartition.[34] Gkeka et al. also carried out a coarse-grained (CG) study on FP membrane insertion compared to different membrane interacting peptide classes.[45] For the SIV FP in CG and atomistic simulations, they found that the peptide tilt distribution was slightly shifted versus a parallel orientation to the membrane surface.[14]

Although these studies appear to support the tilted orientation of FP in membrane, there is not yet any extensive sampling of the peptide configuration in membranes since simulations are generally restrained to tens of nanoseconds with an a priori starting orientation for the fusion peptide. In the study presented here, molecular dynamic simulations with a coarse-grained model (CG-MD) are used to study the configuration of the SIV FP in model bilayers. CG allows one to extend the time and length scale reachable with MD by combining usually 4 heavy atoms in a single CG particle. Sampling without an a priori assumption of peptide orientation is assured by doing 100 simulations of 100 ns in which the bilayer forms itself around the peptide during the first nanoseconds of the simulation. Atomistic simulations of 50 ns have also been performed from selected frames of the CG-MD. The orientation and conformation of WT in membrane, as well as the orientation of mutant FP, are compared to previously predicted and measured values.[29,35]

MATERIAL AND METHODS

Coarse-Grained Simulations. The initial structures of the SIV fusion peptide and mutants (FLG, mutH) have been modeled as all-atom α-helices using standard backbone angles (φ = −60° and ψ = −45°) and side chain conformers.[14,29] These models were converted to a CG representation suitable for the MARTINI forcefield,[46,47] and the coarse-grained peptide was placed in a simulation box (7 × 7 × 9 nm^3) with 126 randomly positioned DPPC or DOPC molecules. The Z dimension was then increased to 15 nm and water particles were added. A 1000-step steepest-descent energy minimization was performed to remove any steric clashes. A bilayer was generated around the peptide by self-assembly.[48] The lipid bilayer is formed during the first nanoseconds of the simulation.[49]

One hundred 0.1 μs simulations have been run for each peptide within the Sidekick high-throughput framework, which was developed to facilitate running large ensembles of simulations in an automated fashion.[49,50] Sidekick automatically monitors whether a simulation successfully completes and whether the bilayer is properly formed. If not, the simulation is restarted. Temperature and pressure were coupled at 323 K for DPPC and 300 K for DOPC and 1 bar using the weak coupling Berendsen algorithm[51] with τ_T = 1 ps and τ_P = 10 ps. Pressure was coupled semi-isotropically in XY and Z. Non-bonded interactions were computed up to 1.2 nm with the shift method. Electrostatics were treated with ε = 15. The compressibility was 3 × 10^5 (1/bar). Coarse-grained simulations have been carried out by using *Gromacs* v 3[52] on a 56-processor Mac OS X cluster. Simulations performed are listed in Table 1. Density profiles have been treated by the multipeak fitting procedure of *QtiPlot 0.9.8* to decompose the curves into Gaussian curves. Membrane surfaces were computed with *GridMat*.[53]

Table 1. Coarse-Grained Simulations Performed

run	system[a]	box size (nm^3)	number of simulations	simulation time (ns)
CG1	SIV WT/DPPC$_{126}$/water	7 × 7 × 15	100	100
CG2	SIV WT/DOPC$_{126}$/water	7 × 7 × 15	100	100
CG3	SIV FLG/DPPC$_{126}$/water	7 × 7 × 15	100	100
CG4	SIV mutH/DPPC$_{126}$/water	7 × 7 × 15	100	100

[a]See Table 3 for the sequences of the peptides.

From Coarse-Grained to Atomistic Model. From the coarse-grained simulations of the SIV FP with DPPC, three different frames have been chosen to carry atomistic simulations. These frames were chosen to catch three different orientations of the SIV peptide in membranes, respectively, with the peptide helix axis parallel (90°), tilted (42°) and perpendicular (4°) to the bilayer normal (Table 2). The

Table 2. Atomistic Simulations Performed

run	system	simulation time (ns)
AT1	SIV WT para/DPPC$_{126}$/water	50
AT2	SIV WT tilt/DPPC$_{126}$/water	50
AT3	SIV WT perp/DPPC$_{126}$/water	50

dx.doi.org/10.1021/jp3027385 | J. Phys. Chem. B 2012, 116, 13713−13721

Table 3. Experimental and in Silico Data from Martin et al.[29]

	sequence	FTIR L/P ratio	predicted orientation (deg)[a]	α helix (%; FTIR data)	FTIR data angle (deg)[a]	fusion (%) (L/P = 23)
SIV WT	GVFVLGFLGFLA	200	37	33 ± 5	40 ± 5	54 ± 3
SIV FLG	GFLGFLAVVFLG	50	45	32 ± 5	45 ± 5	43 ± 3
SIV mutH	FVLGFVGLFLGA	10	81	0		0

[a]Angle vs bilayer normal; predictions have been carried on as described by Brasseur et al.[62]

conversion has been carried out as described in Stansfeld et al. (2009).[54] Briefly, atomistic lipid fragments and amino acid side chains are aligned on the CG particles and Pulchra is used to rebuild the protein backbone from the Cα traces.[55] The energy of the system is then minimized to refine bond lengths and angles and to remove any clashes that resulted from the conversion.

Atomistic Simulations. Simulations have been performed with the GROMOS96 43a1 force field.[56] All the systems studied were first run for a 2 ns simulation with the peptide and lipids under position restraints in periodic boundary conditions (PBC) using a 2 fs time step and then for another 2 ns simulation with the peptide only under position restraints. Production runs were performed for 50 ns (Table 2). All the systems were solvated with SPC water[57] and the dynamics were carried out in the NPT conditions (323 K and 1 bar). Temperature was maintained by using the bath method of Berendsen[51] with τ_T = 1 ps, and a semi-isotropic pressure was maintained by using the Parrinello-Rahman[58] barostat with a compressibility of 4.5 × 10^5 (1/bar) and τ_P = 10 ps. Electrostatic interactions were treated by using the particle mesh Ewald (PME) method. van der Waals and electrostatics were treated with a 1.0 nm cutoff. Bond lengths were maintained with the LINCS algorithm.[59] Positions and velocities of atoms in the system have been saved every 10 ps. All computations were performed on a 30-node dual-core Linux cluster. The trajectories were performed and analyzed with the *GROMACS 4.0.4* tools as well as with homemade scripts and softwares, and 3D structures were analyzed with both *PYMOL*[60] and *VMD*[61] software. Membrane surfaces were computed with *GridMat*.[53]

RESULTS

Coarse-Grained Simulations. In order to obtain better sampling of the interaction between fusion peptides and membrane bilayer, self-assembly simulations have been performed on the SIV fusion peptide and several mutants in a coarse-grained representation. These peptides, listed in Table 3, have been characterized by ATR-FTIR on PC/PE/SM/Chol liposomes by Martin et al.[29] For each peptide, 100 simulations of 100 ns duration were performed and combined for analysis. The angles, measured between the helix axis and the bilayer normal, and distances between the peptide mass center and the bilayer center have been calculated and used to draw the frequency graphs presented in Figure 1. In DPPC, it can be seen that there are two major peptide orientations in the bilayer. One corresponds to an oblique insertion at the phospholipid glycerol level and the other one, less frequent, corresponds to a transmembrane orientation. For the SIV WT, the highest frequency corresponds to an angle of 65° and a peptide-to-bilayer center-to-center distance of 16 Å for the major population and to an angle of 13° and a distance of 1 Å for the minor population. It is worth noting that the peptide can cover a wide range of angles as stated by previous studies.[13,14] As the FTIR orientation values correspond to an

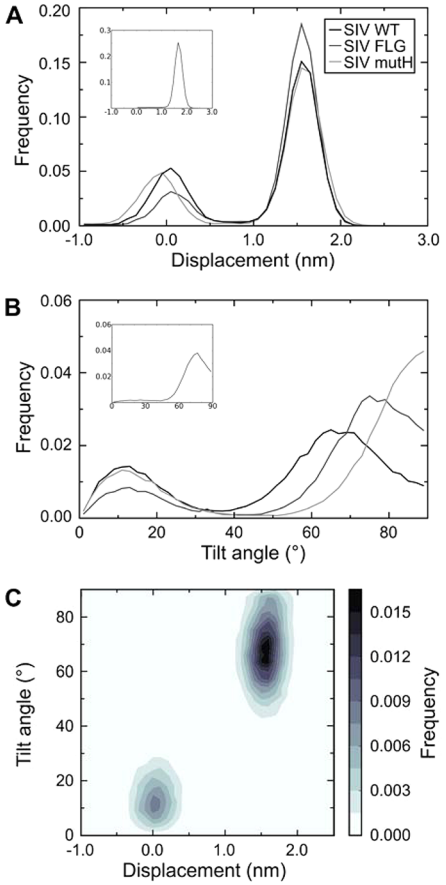

Figure 1. Distribution of the tilt angle (A) and the distances between peptide mass center and bilayer center (B) for coarse-grained simulations of SIV FP WT, FLG, and mutH. These distributions are represented in combination for the SIV FP WT (C). Insets represent the tilt and displacement distributions for DOPC simulations.

average, we can consider the average tilt over the two peptide populations. The average tilt is equal to 53°, which is close to the ATR-FTIR value of 40 ± 5°. For the other peptides, the two populations are also found, suggesting a general behavior for this kind of peptide. For the SIV FLG, which is predicted and measured to be less tilted than the SIV WT fusion peptide, the CG simulations also found this peptide less tilted. The optimal and average tilt values are 75° and 65°, respectively. For the SIV mutH, the optimal tilt is 90° and the average value is 63°. The tilt of the major population actually seems to be related to the fusogenic properties, because the two peptides which induce liposome fusion experimentally are tilted while the other presents an angle of 90°. In DOPC, the SIV fusion peptide also presents a tilted interfacial position (Figure 1). Although present at the beginning of some simulations, the transmembrane position seems not to be as stable as for DPPC. This difference should be due to the restrained secondary structure. As the correlation between the study of Bradshaw et al.[35] and the coarse-grained simulations described in this paper

dx.doi.org/10.1021/jp3027385 | J. Phys. Chem. B 2012, 116, 13713−13721

is very good, the results with DPPC will be used for further calculations.

Regarding the peptide face inserted inside the bilayer for the SIV WT FP, it can be seen from Figure 2A that the major

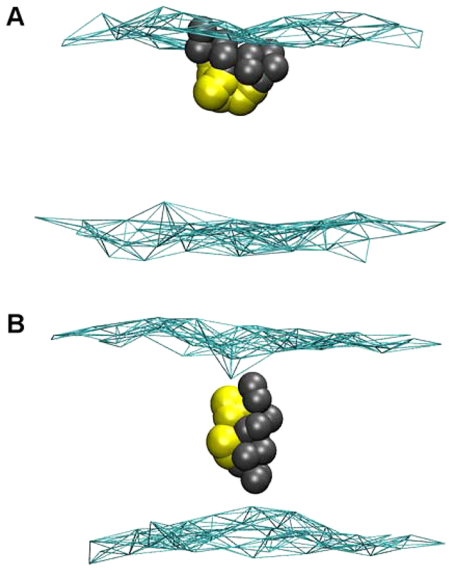

Figure 2. Representative position of the SIV WT peptide for the two populations in DPPC membrane. Backbone particles are gray, Phe side chains are yellow and the bilayer surface (as defined by the phosphate particles) is a gray mesh.

population has the N-terminal end more deeply inserted into the bilayer. The peptide is at the level of glycerol group, with the Phe residues facing the membrane interior. Along the simulations, the peptide presents this configuration, as can be seen in Figure 3B. For the minor population, the peptide is transmembranar and bridges the two sides of the bilayer. As the bilayer thickness is larger than the peptide length, the peptide

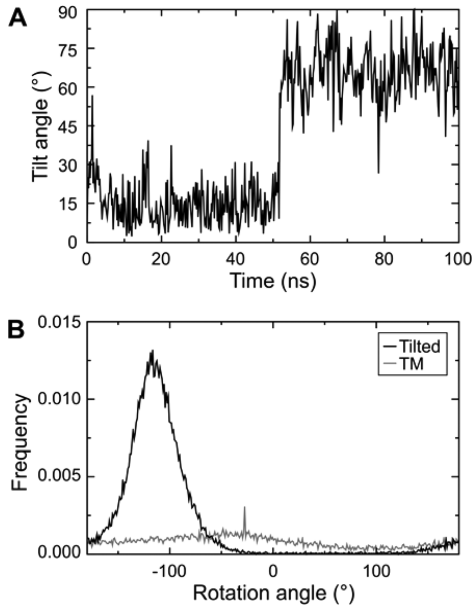

Figure 3. SIV WT angle distribution. (A) Orientation of the helix axis vs the bilayer normal during an individual run and (B) screw rotation of the helix in its tilted and transmembrane (TM) orientations.

pulls some phospholipid heads deeper in the membrane leading to a degree of (local) bilayer thinning. There is no preferential orientation of any helix face for this population in the membrane (Figure 3B).

The membrane thickness, average order parameters, and membrane surface have been computed, and the results are presented as Supporting Information. These results show that the fusion peptides induce a bilayer thinning (Figure S1), with phosphate positions of the lipids closest to the peptide usually being more internal. This effect is evidence for the cis leaflet (containing the peptide) when the peptide is interfacial and for both layers when the peptide is transmembranar. The peptide also has an effect on the lipid ordering. We can distinguish the lipids close to the peptide from those farther away. For the interfacial position, there is a decrease of the value associated with the acyl chain of the cis neighbors. For the transmembrane position, the effect is more important and induces lower values for the cis and trans neighbors. Considering the lipids farther away, the difference observed between the cis and trans leaflets when the peptide is interfacial can be explained by the fact that the surface of the lipid box remains constant. Indeed, there are only 63 lipids per leaflet, while an important area is occupied by interfacial peptide, leading to a decrease of the surface occupied for all lipids of the cis leaflet.

Figure 3A also shows that the peptide can switch between the two populations during the simulations. A transition from TM to the tilted orientation arises in 18% of the simulations, and a transition from the tilt to TM orientation has been observed during one of the 100 simulations.

In 2000, Bradshaw et al. studied the membrane insertion of the SIV FP by neutron diffraction.[35] They also found two populations with two possible orientation models for each population. Regarding their results, they drew density profiles of Val2, Leu8, and Leu11. In the same way, density profiles of these residues have been drawn from our simulations (Figure 4) and the curves broken down into gaussians (Table 4). There are two populations for each residue. A major population representing approximately 70% of the distribution is 13.5−15 Å at the level of the glycerol, depending on the residue, and a minor population (around 30%) corresponding to a deeper position into the membrane. This distribution is very close to what was observed previously.[35] It should be noted that Bradshaw et al. carried out their study in DOPC, so there is a shift along the membrane axis. In both studies, peptides from the major population are at the hydrophobic/hydrophilic interface and the shift can be seen on the Table 4. For the minor population, Leu8 and Leu11 are inserted more deeply into the membrane in our simulations, the peptides being transmembranar instead of tilted as observed experimentally. This explains the difference of the value in Table 4. We assume that the peptide is probably transmembranar in the CG simulation instead of tilted because of the shorter thickness of the DPPC vs DOPC membrane.

Atomistic Simulations. From the coarse-grained simulations of SIV FP in DPPC, we carried out atomistic simulations of 50 ns duration starting from three different orientations, i.e., interfacial (AT1), interfacial-oblique (AT2), or transmembrane (AT3). These simulations were carried out to follow the peptide behavior in an atomistic representation without restraints on the conformation. When starting from an interfacial orientation, the peptide stays in a helical conformation and becomes slightly tilted. The angle distribution is close to that obtained with the coarse-grained simulations with

dx.doi.org/10.1021/jp3027385 | J. Phys. Chem. B 2012, 116, 13713−13721

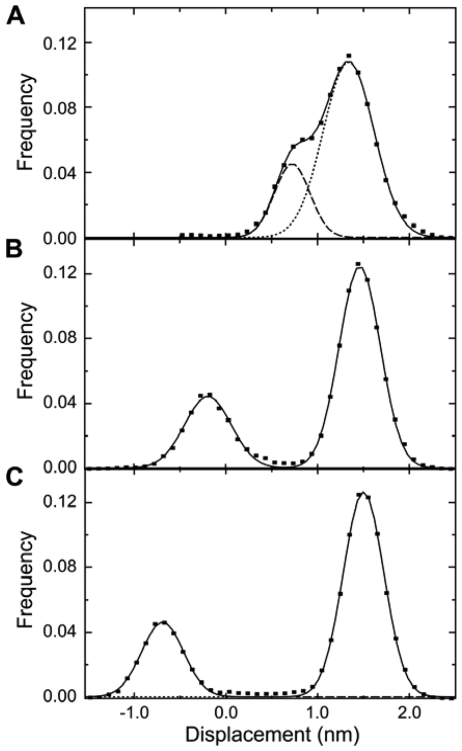

Figure 4. Density profiles of the Val2 (A), Leu8 (B), and Leu11 (C) relative to the bilayer center.

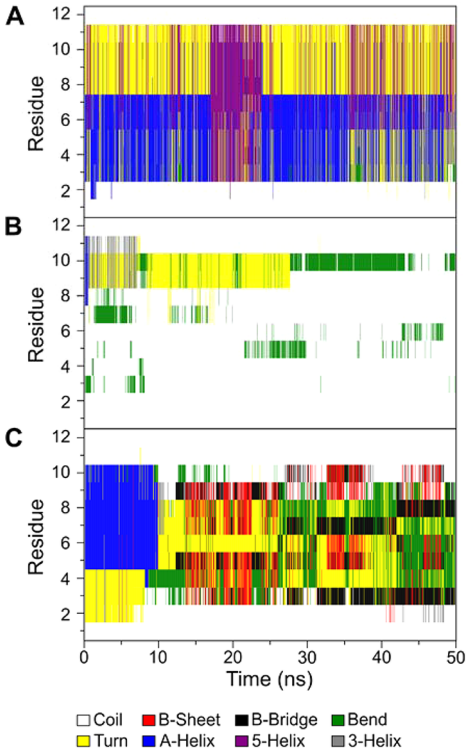

Figure 5. Secondary structure for atomistic simulations of SIV FP (A) AT1, (B) AT2, and (C) AT3.

a distribution presenting a maximum at 77° (Figure 6). With AT3, the peptide tends to stay in a nearly transmembrane configuration, but after 10 ns, it loses helical conformation and becomes β sheet (Figure 5). With AT2, the peptide unfolds.

Figure 6 shows that the SIV FP is embedded within the acyl chains regardless of the orientation or structure. The peptide seems to insert more deeply into the membrane in the atomistic than in the CG simulation: for example, at 9 Å for AT1 instead of 15 Å for CG. By comparing AT1 and 2, we observe that the peptide penetrates more deeply into the membrane when helical. For AT3, the peptide evolves around the membrane center.

Snapshots have been taken from the simulations to illustrate the membrane insertion (Figure 7). For AT1 (Figure 7A), the phenyl groups are thought to push the peptide within the membrane while the N-terminal amide group preferentially interacts with carbonyl groups and water. For AT3 (Figure 7B), the transmembrane orientation is associated with a curvature in the membrane and the presence of water in the bilayer. The β-structure is well-illustrated in Figure 7B.

Regarding the membrane thickness, average order parameters, and membrane surface for atomistic simulations, the differences between the different conformations are clearer. A thinning can be observed for the layer containing the WT peptide and for both layers when the peptide is in a transmembrane position (Figure S4). This thinning is also observed in Figure S6. Regarding the order parameters, the values are similar to those of Volnisky et al. (2005) with lower values for lipid chains of the molecules close to the peptide. This effect is also more important for the helical peptide than for the random coil peptide. For the transmembane peptide, the effect is similar as in CG with lower values for the cis and trans neighbors.

Table 4. Gaussian Parameters for the Density Profiles of the Val2, Leu8, and Leu11

		coarse grained			neutron diffraction		
peak	parametrer	valine 2	leucine 8	leucine 11	valine 2	leucine 8	leucine 11
1	position[a]	13.5 Å	14.7 Å	15.0 Å	19.9 Å	18.6 Å	16.5 Å
	width[b]	5.5 Å	4.4 Å	4.4 Å	17.3 Å	6.5 Å	12.6 Å
	distribution[c]	77%	71%	73%	74 ± 13%	76 ± 6%	82 ± 8%
2	position[a]	7.4 Å	−1.7 Å	−6.7 Å	10.5 Å	7.4 Å	4.8 Å
	width[b]	3.8 Å	5.0 Å	4.5 Å	14.3 Å	3.2 Å	6.3 Å
	distribution[c]	23%	29%	27%	26 ± 13%	24 ± 6%	18 ± 8%
	error[d]	5.8%	6.2%	6.5%	1.9%	1.0%	1.1%

[a]Position of the peak relative to the bilayer center. [b]The width corresponds to two standard deviations (σ) and is approximately 0.849 of the peak width at half height. [c]Percentage of area under the curve. [d]The error corresponds to the sum of the absolute differences between the Gaussian curve and observed values.

dx.doi.org/10.1021/jp3027385 | J. Phys. Chem. B 2012, 116, 13713−13721

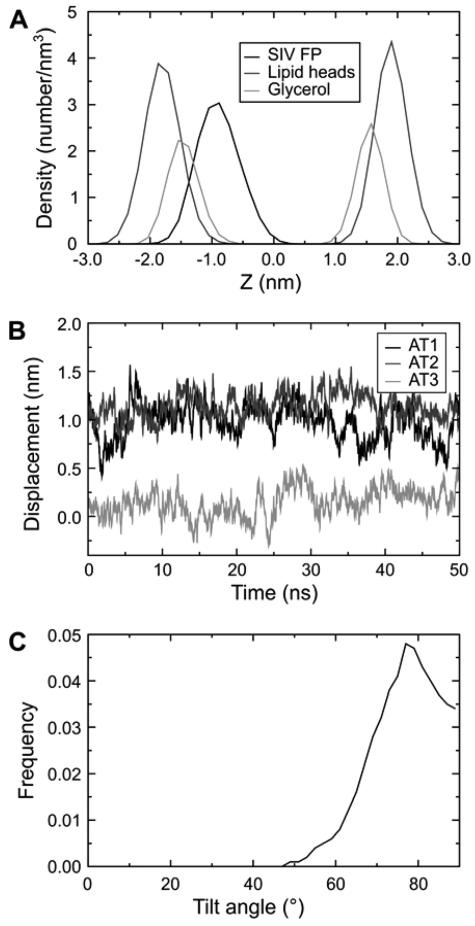

Figure 6. (A) Density profiles of the SIV FP, lipid heads, and Glycerol for AT1; Glycerol is represented by the central carbon and the lipid heads by phosphorus and nitrogen of the phosphocholine group. (B) Position of the SIV FP in the membrane. (C) Distribution of the tilt angle for AT1.

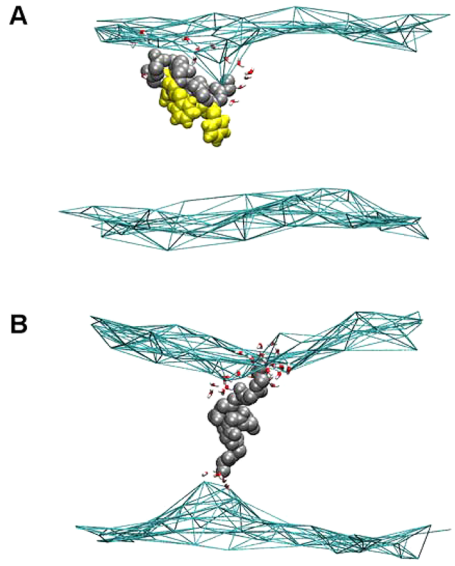

Figure 7. Snapshots representative of the atomistic simulations (A, AT1 at 4.5 ns; and B, AT3 at 27 ns). Backbone particles are gray, Phe side chains are yellow, and the bilayer surface (as defined by the phosphate particles) is a gray mesh. Water molecules within 5 Å of the peptide are also represented.

DISCUSSION

Coarse-grained molecular dynamics simulations enable improved sampling of peptide−membrane interactions. Furthermore, with the self-assembly protocol, there is no a priori bias on the initial peptide orientation in the membrane. This technique has been used here to study the interaction between the SIV FP and DPPC and DOPC bilayers. The simulations mainly indicate that the SIV fusion peptide can adopt two different orientations in a DPPC bilayer, with a major population presenting a tilt relative to the bilayer normal and a minor population which is parallel to the membrane normal. To compare our results to the ATR-FTIR values, we computed the average tilt over the two populations, since in this experimental technique, the angles measured correspond to an average value.[29] As already mentioned, there is a very good agreement between both values (53° vs 45°). It should be noted that, due to this averaging, two populations cannot be distinguished by infrared spectroscopy. Contrary to ATR-FTIR, two sets of peptide with different tilt angles and depth of penetration have been observed by neutron diffraction.[35] Moreover, when we compare the position distribution of SIV residues Val2, Leu8, and Leu11, there is a good correlation between the two approaches. Concerning the peptide tilt in the membrane, Bradshaw et al. have also observed two populations, each corresponding to two possible models regarding their results.[35] An angle of 78° and 55° was possible for the major population and an angle of 85° and 50° for the minor one. On the basis of previous studies, they stated that the most plausible model corresponds to the model with an angle of 55° (stated as model B in their publication). Since our results are very close to those of Bradshaw, we can decipher between the two possible configurations of each population. For the major one, we observe a tilt of 65°, the N-terminal end being inserted deeper and Leu11 facing the membrane core. This position matches the Bradshaw A model (78°). For the minor population, the distribution (%) is similar, but peptide orientations between the two studies are different. The minor population is transmembranar in the CG study and described as tilted in the neutron diffraction assays. This should be due to the different lipids used, DPPC for CG-MD and DOPC for neutron diffraction. The CG-MD simulations with DOPC are similar to those with DPPC but without the transmembrane orientation. This difference should be due to the restrained secondary structure and should probably disappear in AT simulations. The DPPC bilayer is thinner and allows a stable transmembrane position for the SIV FP, which should not be favored in DOPC. Gkeka et al. performed a CG-MD study of the SIV FP in DOPC: they observed an optimal localization of the peptide at the membrane interface and indicated that more internal positions were possible though less preferred.[45] Although we have not observed this more internal position, this could also be in agreement with the presence of a minor population more deeply inserted in the membrane as seen by Bradshaw.[35] Regarding the peak width, Bradshaw et al. suggested that the peaks of Val2 and Leu11 are broader than the peak of Leu8 because the peptide structure should be more random at the terminus. For the coarse-grained study, restraints are applied on the secondary structure of the peptide and this could explain why these peaks are thinner in the simulations. To compare the effect of the lipid heads, CG simulations have also been made with DPPE (data not shown). PE has a smaller head than PC and has been shown to be important in helping the fusion

process in vitro. The peptide presents the same behavior in either lipid.

The order parameter cannot distinguish between the WT and the mutants, as the same effects are observed for the three peptides (see Figures S1 and S2). The discrimination is mainly evidenced by the clear difference in the tilt and depth of penetration, as shown on Figure S3. We assume that a more important tilt could induce a greater thinning of the membrane. As the wild-type peptide is the most tilted, it would also have the greatest effect on the membrane.

In agreement with the results of Lins et al., the study also shows that the peptide has access to a wide range of tilt angles, from 0° to 50°,[14] the optimal position corresponding to an angle of 37° and 8 Å for the depth of insertion.[14] As suggested by that study,[14] this position corresponds to the minor population observed by Bradshaw et al., which penetrates at the level of the lipid acyl chains. It should be noted that, in the simulations published in ref 14, the membrane was implicitly represented. The presence of lipid molecules in the simulation appears to favor a more interfacial tilted position.

The CG simulations show that for the SIV mutant which does not induce fusion in vitro the major population is no more tilted, indicating a relation between fusogenicity and tiltedness, as previously noticed.[29] It should be noted that the difference observed for the insertion between WT and mutants in the simulations and for fusion in the experimental assays cannot be due to a difference in hydrophobicity because the mutants are obtained by residue permutation and hence have the same amino acid composition. For the SIV mutH, the CG results indicate a marked preference of this peptide to lay parallel at the membrane surface even if the average value between the two populations is equal to 63°. The main orientation is in agreement with the previous model that has been predicted with an angle around 80°. It should be mentioned that there is a lack of experimental value for the angle of this mutant, since it has been found to adopt a β-conformation.

Regarding the conformation, most of the molecular dynamics studies on fusion peptides have postulated a helical conformation, which seemed to remain stable during the course of the simulations.[32,37−40,42,45] Taking those studies into account, this conformation was also used here. Experimentally, Martin et al. observed a mix of secondary structure for the SIV FP peptide in presence of lipids. They suggested that the peptide should be present under two major conformations in their experiments: a mainly β-strand population and another mainly helical. Compared to CG-MD which involve restraints on secondary structure, our atomistic simulations show that the peptide can adopt the different conformations observed by ATR-FTIR. Three main situations are observed: the peptide can be destructured at the membrane surface, tilted within the membrane when helical, or can adopt a β-structure when perpendicular to the membrane. When helical, the peptide presents a similar orientation in the CG and atomistic simulations. Martin et al. have observed the SIV FP as mainly β-sheet in solution. Our simulations suggest that the peptide could also adopt this structure inside the membrane. As postulated by Charloteaux et al., the peptide could oligomerize as a β-sheet structure during the formation of the fusion pore. It is worth noting that the simulations show that the SIV FP induces a perturbation of the surrounding phospholipids, with some lipid heads and water being pushed inside the membrane. This effect is even more important when the peptide is transmembrane and β-conformed. Moreover, although the peptides are in different conformations, the density profiles of Val2, Leu8, and Leu11 for the transmembrane orientation in the coarse-grained and AT simulations (Figure S7) show similar positions. The tilted orientation of the FPs has been observed and discussed by many computational and experimental studies and it appears responsible for their lipid destabilizing activity (for a review, see Charloteaux et al.[5]). We and others have suggested that the oblique insertion into the membrane disturbs the organization of the lipid acyl chains and expands the region in the center of the bilayer.[4,5,18] This is consistent with the appearance of a negative curvature observed experimentally. A number of fusion peptides notably lower the bilayer to hexagonal phase transition temperature of phosphatidylethanolamine.[4,63] Promotion of a negative curvature is involved in the formation of hemifusion intermediate.[7,64] Fusion peptides could also lower the rupture tension of membranes as has been observed experimentally for the influenza fusion peptide.[65] This peptide can also promote the formation of cubic phases and it has recently been observed by CG-MD that the influenza FP spontaneously induces a bicontinuous cubic phase. Fusion peptides could then lower fusion intermediate energies and be implicated at different stages of the membrane fusion.[64,66,67]

CONCLUSION

Our simulations present a very good correlation with previous experimental studies and the tilted configuration of fusion peptides. The distribution and orientation of the peptide are similar to what was observed by neutron diffraction, and the simulations helped to decipher among the different orientations described by Bradshaw et al.[35] Moreover, when converted from a coarse-grained to all-atom model, the simulations showed that the fusion peptide under a tilted and helical conformation corresponds to a stable configuration, further validating the tilted peptide model. The coarse-grained simulations also exhibit a good correlation with the mean angles determined by ATR-FTIR. The results obtained for the non-fusogenic mutants further support a correlation between the tilted insertion of the peptide and its fusogenic properties, as previously suggested.[29]

ASSOCIATED CONTENT

Supporting Information

Figure S1: Time evolution of the bilayer thickness for SIV WT (A and D), SIV FLG (B and E) and SIV mutH (C and F) in an interfacial (A, B and C) or transmembrane (D, E and F) orientation. The bilayer thickness is measured between averaged cis (leaflet containing the peptide) and trans phosphate groups and between the 10 first phosphate neigbours for the cis and trans leaflet. Figure S2: Average order parameters (S_{cd}) for CG simulations with SIV WT (A and D), SIV FLG (B and E) and SIV mutH (C and F) with an interfacial (A, B and C) or transmembrane orientation (D, E and F) of the peptides. Figure S3: Landscapes of the membrane surfaces for the SI WT peptide at an angle of 13° (A), 45° (B), 65° (C) and 90° (D). Figure S4: Time evolution of the bilayer thickness for the AT simulations (A) AT1 (B) AT2 and (C) AT3. The bilayer thickness is measured between averaged cis (leaflet containing the peptide) and trans phosphate groups and between the 10 first phosphate neigbours for the cis and trans leaflet. Figure S5: Average order parameters (S_{cd}) for DPPC acyl chains of the AT simulations (A) AT1 (B) AT2 and (C) AT3. Order parameters are computed for the cis (containing the peptide) and trans leaflets and for the 10 closest lipids of

the cis and trans leaflet. Figure S6: Landscapes of the membrane surfaces for AT1 (A), AT2 (B) and AT3 (C). Figure S7: Density profiles of the Val 2 (A), Leu 8 (B) and Leu 11 (C) relative to the bilayer center for the AT3 simulation. This material is available free of charge via the Internet at http://pubs.acs.org.

AUTHOR INFORMATION

Corresponding Author

*Telephone: 32-81-622521. Fax: 32-81-622522. E-mail: jmcrowet@ulg.ac.be.

Present Addresses

[§]Department of Chemistry, University of Chicago, 5735 South Ellis Avenue, Chicago, Illinois 60637.

[∥]Centre for Computational Science, Department of Chemistry, University College London, 20 Gordon St, London, WC1H 0AJ, United Kingdom.

Author Contributions

[#]Equal contributors.

Notes

The authors declare no competing financial interest.

ACKNOWLEDGMENTS

J.M.C. is supported by the Belgian Program on Interuniversity Attraction Poles initiated by the Federal Office for Scientific, Technical and Cultural Affairs (IAP. P6/19 PROFUSA). L.L. is senior research associate and R.B. is a research director for the Fonds National pour la Recherche Scientifique (FNRS, Belgium). Research in M.S.P.S.'s laboratory is funded by BBSRC and the Wellcome Trust. We also thank the ERASMUS STT program.

REFERENCES

(1) Earp, L. J.; Delos, S. E.; Park, H. E.; White, J. M. *Curr. Top. Microbiol. Immunol.* **2005**, *285*, 25−66.

(2) Kowalski, M.; Potz, J.; Basiripour, L.; Dorfman, T.; Goh, W. C.; Terwilliger, E.; Dayton, A.; Rosen, C.; Haseltine, W.; Sodroski, J. *Science* **1987**, *237*, 1351−1355.

(3) Lasky, L. A.; Nakamura, G.; Smith, D. H.; Fennie, C.; Shimasaki, C.; Patzer, E.; Berman, P.; Gregory, T.; Capon, D. J. *Cell* **1987**, *50*, 975−985.

(4) Epand, R. M. *Biochim. Biophys. Acta* **2003**, *1614*, 116−121.

(5) Charloteaux, B.; Lorin, A.; Brasseur, R.; Lins, L. *Protein Pept. Lett.* **2009**, *16*, 718−725.

(6) Martin, I. I.; Ruysschaert, J.; Epand, R. M. *Adv. Drug Delivery Rev.* **1999**, *38*, 233−255.

(7) Chernomordik, L. V.; Kozlov, M. M. *Nat. Struct. Mol. Biol.* **2008**, *15*, 675−683.

(8) Horth, M.; Lambrecht, B.; Khim, M. C.; Bex, F.; Thiriart, C.; Ruysschaert, J. M.; Burny, A.; Brasseur, R. *EMBO J.* **1991**, *10*, 2747−2755.

(9) Luneberg, J.; Martin, I.; Nussler, F.; Ruysschaert, J. M.; Herrmann, A. *J. Biol. Chem.* **1995**, *270*, 27606−27614.

(10) Brasseur, R.; Lorge, P.; Goormaghtigh, E.; Ruysschaert, J. M.; Espion, D.; Burny, A. *Virus Genes* **1988**, *1*, 325−332.

(11) Brasseur, R.; Vandenbranden, M.; Cornet, B.; Burny, A.; Ruysschaert, J. M. *Biochim. Biophys. Acta* **1990**, *1029*, 267−273.

(12) Brasseur, R. *J. Biol. Chem.* **1991**, *266*, 16120−16127.

(13) Efremov, R. G.; Nolde, D. E.; Volynsky, P. E.; Chernyavsky, A. A.; Dubovskii, P. V.; Arseniev, A. S. *FEBS Lett.* **1999**, *462*, 205−210.

(14) Lins, L.; Charloteaux, B.; Thomas, A.; Brasseur, R. *Proteins* **2001**, *44*, 435−447.

(15) Voneche, V.; Portetelle, D.; Kettmann, R.; Willems, L.; Limbach, K.; Paoletti, E.; Ruysschaert, J. M.; Burny, A.; Brasseur, R. *Proc. Natl. Acad. Sci. U.S.A.* **1992**, *89*, 3810−3814.

(16) Pillot, T.; Goethals, M.; Vanloo, B.; Talussot, C.; Brasseur, R.; Vandekerckhove, J.; Rosseneu, M.; Lins, L. *J. Biol. Chem.* **1996**, *271*, 28757−28765.

(17) Pillot, T.; Lins, L.; Goethals, M.; Vanloo, B.; Baert, J.; Vandekerckhove, J.; Rosseneu, M.; Brasseur, R. *J. Mol. Biol.* **1997**, *274*, 381−393.

(18) Brasseur, R. *Mol. Membr. Biol.* **2000**, *17*, 31−40.

(19) Colotto, A.; Martin, I.; Ruysschaert, J. M.; Sen, A.; Hui, S. W.; Epand, R. M. *Biochemistry* **1996**, *35*, 980−989.

(20) Korazim, O.; Sackett, K.; Shai, Y. *J. Mol. Biol.* **2006**, *364*, 1103−1117.

(21) Pereira, F. B.; Goni, F. M.; Muga, A.; Nieva, J. L. *Biophys. J.* **1997**, *73*, 1977−1986.

(22) Yang, J.; Gabrys, C. M.; Weliky, D. P. *Biochemistry* **2001**, *40*, 8126−8137.

(23) Li, Y.; Tamm, L. K. *Biophys. J.* **2007**, *93*, 876−885.

(24) Reichert, J.; Grasnick, D.; Afonin, S.; Buerck, J.; Wadhwani, P.; Ulrich, A. S. *Eur. Biophys. J.* **2007**, *36*, 405−413.

(25) White, J. M.; Delos, S. E.; Brecher, M.; Schornberg, K. *Crit. Rev. Biochem. Mol. Biol.* **2008**, *43*, 189−219.

(26) Decout, A.; Labeur, C.; Vanloo, B.; Goethals, M.; Vandekerckhove, J.; Brasseur, R.; Rosseneu, M. *Mol. Membr. Biol.* **1999**, *16*, 237−246.

(27) Lins, L.; Flore, C.; Chapelle, L.; Talmud, P. J.; Thomas, A.; Brasseur, R. *Protein Eng.* **2002**, *15*, 513−520.

(28) Castano, S.; Desbat, B. *Biochim. Biophys. Acta* **2005**, *1715*, 81−95.

(29) Martin, I.; Dubois, M. C.; Defrise-Quertain, F.; Saermark, T.; Burny, A.; Brasseur, R.; Ruysschaert, J. M. *J. Virol.* **1994**, *68*, 1139−1148.

(30) Martin, I.; Schaal, H.; Scheid, A.; Ruysschaert, J. M. *J. Virol.* **1996**, *70*, 298−304.

(31) Perez-Mendez, O.; Vanloo, B.; Decout, A.; Goethals, M.; Peelman, F.; Vandekerckhove, J.; Brasseur, R.; Rosseneu, M. *Eur. J. Biochem.* **1998**, *256*, 570−579.

(32) Kamath, S.; Wong, T. C. *Biophys. J.* **2002**, *83*, 135−143.

(33) Peuvot, J.; Schanck, A.; Lins, L.; Brasseur, R. *J. Theor. Biol.* **1999**, *198*, 173−181.

(34) Taylor, A.; Sansom, M. S. *Eur. Biophys. J.* **2010**, *39*, 1537−1545.

(35) Bradshaw, J. P.; Darkes, M. J.; Harroun, T. A.; Katsaras, J.; Epand, R. M. *Biochemistry* **2000**, *39*, 6581−6585.

(36) Han, X.; Bushweller, J. H.; Cafiso, D. S.; Tamm, L. K. *Nat. Struct. Biol.* **2001**, *8*, 715−720.

(37) Huang, Q.; Chen, C. L.; Herrmann, A. *Biophys. J.* **2004**, *87*, 14−22.

(38) Volynsky, P. E.; Polyansky, A. A.; Simakov, N. A.; Arseniev, A. S.; Efremov, R. G. *Biochemistry* **2005**, *44*, 14626−14637.

(39) Lague, P.; Roux, B.; Pastor, R. W. *J. Mol. Biol.* **2005**, *354*, 1129−1141.

(40) Vaccaro, L.; Cross, K. J.; Kleinjung, J.; Straus, S. K.; Thomas, D. J.; Wharton, S. A.; Skehel, J. J.; Fraternali, F. *Biophys. J.* **2005**, *88*, 25−36.

(41) Vaidya, N. K.; Huang, H.; Takagi, S. *Adv. Appl. Math. Mech.* **2010**, *2*, 430−450.

(42) Wong, T. C. *Biochim. Biophys. Acta* **2003**, *1609*, 45−54.

(43) Li, J.; Das, P.; Zhou, R. *J. Phys. Chem. B* **2010**, *114*, 8799−8806.

(44) Kasson, P. M.; Lindahl, E.; Pande, V. S. *PLoS Comput. Biol.* **2010**, *6*, e1000829.

(45) Gkeka, P.; Sarkisov, L. *J. Phys. Chem. B* **2010**, *114*, 826−839.

(46) Marrink, S. J.; Risselada, H. J.; Yefimov, S.; Tieleman, D. P.; de Vries, A. H. *J. Phys. Chem. B* **2007**, *111*, 7812−7824.

(47) Monticelli, L.; Kandasamy, S. K.; Periole, X.; Larson, R. G.; Tieleman, D. P.; Marrink, S. J. *J. Chem. Theory Comput.* **2008**, *4*, 819−834.

(48) Bond, P. J.; Sansom, M. S. *J. Am. Chem. Soc.* **2006**, *128*, 2697−2704.

(49) Vostrikov, V. V.; Hall, B. A.; Greathouse, D. V.; Koeppe, R. E., 2.; Sansom, M. S. *J. Am. Chem. Soc.* **2010**, *132*, 5803−5811.

(50) Hall, B. A.; Chetwynd, A. P.; Sansom, M. S. P. *Biophys. J.* **2011**, *100*, 1940−1948.
(51) Berendsen, H. J. C.; Postma, J. P. M.; van Gunsteren, W. F.; DiNola, A.; Haak, J. R. *J. Chem. Phys.* **1984**, *81*, 3684−3690.
(52) Lindahl, E.; Hess, B.; van der Spoel, D. *J. Mol. Model.* **2001**, *7*, 306−317.
(53) Allen, W. J.; Lemkul, J. A.; Bevan, D. R. *J. Comput. Chem.* **2009**, *30*, 1952−1958.
(54) Stansfeld, P. J.; Hopkinson, R.; Ashcroft, F. M.; Sansom, M. S. *Biochemistry* **2009**, *48*, 10926−10933.
(55) Rotkiewicz, P.; Skolnick, J. *J. Comput. Chem.* **2008**, *29*, 1460−1465.
(56) Scott, W. R. P.; Hunenberger, P. H.; Tironi, I. G.; Mark, A. E.; Billeter, S. R.; Fennen, J.; Torda, A. E.; Huber, T.; Kruger, P.; van Gunsteren, W. F. *J. Phys. Chem. A* **1999**, *103*, 3596−3607.
(57) Hermans, J.; Berendsen, H. J. C.; Van Gunsteren, W. F.; Postma, J. P. M. *Biopolymers* **1984**, *23*, 1513−1518.
(58) Parrinello, M.; Rahman, A. *J. Appl. Phys.* **1981**, *52*, 7182−7190.
(59) Hess, B.; Bekker, H.; Berendsen, H. J. C.; Fraaije, J. *J. Comput. Chem.* **1997**, *18*, 1463−1472.
(60) *The PyMOL Molecular Graphics System*, version 1.3; Schrödinger, LLC.
(61) Humphrey, W.; Dalke, A.; Schulten, K. *J. Mol. Graph.* **1996**, *14* (33−8), 27−8.
(62) Brasseur, R. In *Molecular description of biological membrane components by computer aided conformational analysis*, Brasseur, R., Ed.; CRC Press Inc.: Boca Raton, 1990; pp 95−105.
(63) Epand, R. *Biochim. Biophys. Acta* **1998**, *1376*, 353−368.
(64) Siegel, D. *Biophys. J.* **1999**, *76*, 291−313.
(65) Longo, M.; Waring, A.; Hammer, D. *Biophys. J.* **1997**, *73*, 1430−1439.
(66) Fuhrmans, M.; Knecht, V.; Marrink, S. J. *J. Am. Chem. Soc.* **2009**, *131*, 9166−9167.
(67) Siegel, D.; Epand, R. *Biochim. Biophys. Acta* **2000**, *1468*, 87−98.